

Scaling of fluid flow versus fracture stiffness

Christopher L. Petrovitch,¹ David D. Nolte,¹ and Laura J. Pyrak-Nolte^{1,2,3}

Received 30 January 2013; revised 12 April 2013; accepted 15 April 2013; published 31 May 2013.

[1] Seismic characterization of fluid flow through fractures requires a fundamental understanding of the relationship between the hydraulic and mechanical properties of fractures. A finite-size scaling analysis was performed on fractures with weakly correlated random aperture distributions to determine the fundamental scaling relationship between fracture stiffness and fracture fluid flow. From computer simulations, the dynamic transport exponent, which provides the power law dependence, was extracted and used to collapse the flow-stiffness relationships from multiple scales into a single scaling function. Fracture specific stiffness was determined to be a surrogate for void area that is traditionally used in percolation studies. The flow-stiffness scaling function displays two exponentially dependent regions above and below the transition into the critical regime. The transition is governed by the stressed flow paths when the flow path geometry deforms from a sheet-like topology to a string-like topology. The resulting hydromechanical scaling function provides a link between fluid flow and the seismic response of a fracture. **Citation:** Petrovitch, C. L., D. D. Nolte, and L. J. Pyrak-Nolte (2013), Scaling of fluid flow versus fracture stiffness, *Geophys. Res. Lett.*, 40, 2076–2080, doi:10.1002/grl.50479.

1. Introduction

[2] A non-intrusive geophysical technique to probe the hydraulic properties of rock fractures has long been sought by scientists and engineers. Such a technique would provide a new method to ascertain the effectiveness of subsurface projects such as the extraction of drinkable water, production of oil and petroleum, installation and monitoring of subsurface infrastructure, and the storage of anthropogenic byproducts (CO₂, nuclear waste, etc.) in subsurface reservoirs. Extensive research has been performed on the laboratory scale to examine fluid flow through fractures, fracture geometry, and deformation under stress as well as the seismic response of fractures. However, one of the fundamental tasks in geophysics is to relate fracture properties and processes at one length scale to properties and processes at other length scales. For example, in the laboratory, measurements are performed on fractured rock samples that range in size from 10⁻² to 10⁻¹ m with fracture apertures on the order of

10⁻⁶ to 10⁻⁴ m using seismic wavelengths on the order of 10⁻³ to 10⁻² m. Conversely, at field scales, seismic frequencies from 1 Hz to 1 kHz illuminate regions on the order of 10³ to 10¹ m. Thus, the development of seismic methods that can delineate and characterize the hydraulic properties of fractures requires a fundamental understanding of the relationship between the hydraulic and mechanical properties of fractures and how this relationship scales with the size of the sampled region.

[3] The ability to relate and scale the hydromechanical properties of fractures requires that both hydraulic and mechanical processes are controlled at similar length scales associated with fracture geometry (e.g., size and spatial distributions of aperture and contact area, surface roughness, fracture length, etc.). There have been many attempts to quantify the role of these geometric quantities with regard to fluid flow and deformation as a function of stress. For instance, *Witherspoon et al.* [1980] showed that the flow rates associated with fractures under normal load have three distinct behaviors as a function of stress. At low stresses, flow rates obey the “cubic” law. However, as normal stress increases, the flow rate deviates from the cubic-law aperture dependence. Deviations from the cubic law were partially explained by using the dominant surface roughness wavelength to approximate the hydraulic aperture [*Zimmerman et al.*, 1990; *Zimmerman and Bodvarsson*, 1996]. Alternatively, a correction factor was constructed from the ratio of the first and second moments of the aperture distribution [*Renshaw*, 1995]. While these approaches focused on the void areas across the fracture plane, the contact area provides another approach. The fracture was modeled as a system of interacting circular obstructions confined to a plane [*Walsh*, 1981]. The analytic solution for the flow around a circular obstruction was used to compute the total flow rate through the fracture. This approach provided a stress-dependent flow rate, but the contact area was assumed to increase linearly with stress [*Walsh and Grosenbaugh*, 1979].

[4] It has been shown experimentally that, at high stresses, the flow exponent deviates from the “cubic” law due to the deformation of the fracture void geometry. Metal castings of natural granite fractures were made at stresses as high as 85 MPa. The castings showed large regions of void space connected by narrow tortuous channels [*Pyrak-Nolte et al.*, 1987; *Jaeger et al.*, 2007]. This experiment found that the large void spaces deformed significantly as the normal load increased, while narrow channels remained open because they were supported by adjacent contact area. From these observations, the authors concluded that once the narrow paths dominate the fluid flow, the flow becomes approximately independent of stress. Following this study, a more unified numerical approach was taken that included both mechanical deformation and fluid flow [*Pyrak-Nolte and Morris*, 2000]. Experimental flow-stiffness data for

¹Department of Physics, Purdue University, West Lafayette, Indiana, USA.

²Department of Civil Engineering, Purdue University, West Lafayette, Indiana, USA.

³Department of Earth and Atmospheric Science, Purdue University, West Lafayette, Indiana, USA.

Corresponding author: C. L. Petrovitch, Department of Physics, Purdue University, West Lafayette, IN 47907, USA. (cpetrovi@purdue.edu)

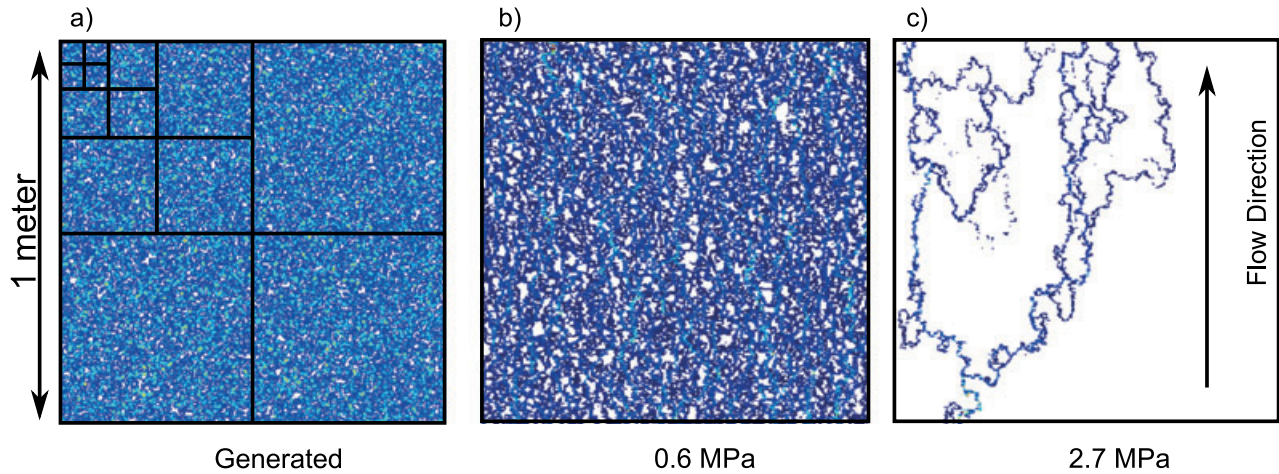


Figure 1. (a) An example of a simulated weakly correlated fracture with an average aperture of 20 microns. The lines indicate the finite-sized subsamples. (b) Fluid velocity field at 0.6 MPa. (c) The same fracture fluid velocity field at 2.7 MPa normal load.

fractures that ranged in length from 0.05 m to 0.3 m suggested an empirical relationship between the hydraulic and mechanical properties that appeared to be controlled by the geometry of the void spaces and the contact area in the fracture. A strong dependence of flow on stiffness was observed, but the samples had different aperture distributions and scale. An outstanding question is whether there exists a scaling relationship between flow and stiffness when appropriate geometric length scales are taken into consideration.

[5] In this letter, a finite-size scaling approach is presented that quantifies the scaling relationship between fluid flow and fracture specific stiffness for single fractures with weakly correlated random aperture distributions. The scale-dependence is removed by finding the critical transport scaling exponent that yields a scaling function.

2. Methods

[6] Fractures with edge lengths that range from 0.0625 to 1 m were simulated to span over an order of magnitude in length scale. A larger range in scale would be preferred, but is not computationally feasible at this time. By allowing the fracture size to vary, the data were expected to display both *critical* and *effective medium* regimes. A fracture is in the effective medium regime when the scaling of fluid flow can be described completely through the moments of the aperture distribution. It is in the critical regime when flow paths are tenuous, and flow is a non-trivial function of the scale and topology. To quantify these two regimes, percolation theory uses the void area fraction as the critical variable. In the critical regime, the flow-stiffness relation can be written in a finite-size scaling form as

$$q \propto L^{-t/\mu} F[(\kappa - \kappa_c)L^{1/\mu}] \quad (1)$$

where q , κ , κ_c and L are the flow rate, fracture specific stiffness, critical specific stiffness, and scale, respectively. The exponents, μ and t , are the 2D correlation exponent and the dynamic flow exponent, respectively. The 2D correlation exponent has a well-known value of $4/3$ [Stauffer and Aharony, 1985], but the flow exponent must be determined numerically. The function F is possibly a scaling function that also must be obtained numerically. The critical specific

stiffness is defined as the stiffness of a fracture when the normal load has reduced the void area fraction to the critical area percolation threshold. If the sample size is at the infinite limit, flow would reduce to zero at the critical stiffness. For finite sample sizes, finite-size effects result in non-zero flow at the critical stiffness. Flow has the form of a power-law as the stiffness approaches the critical stiffness because the function F approaches a constant.

[7] Three computational methods were used to study the flow-stiffness relationship: (1) a numerical approach to generate aperture-scale (10 to 100 microns) fracture void geometry for fractures that span over an order of magnitude in fracture length (0.0625 to 1 m); (2) a combined conjugate-gradient solver and fast-multipole method for determining fracture deformation; and (3) a flow network model for simulating fluid flow, fluid velocity, and fluid pressures within a fracture. To generate a fracture void geometry, the fracture plane was defined as a 512×512 array of pixels. Within this array, a “point” represented by 4×4 pixels was randomly added to the array (incrementing aperture by 1). Each pixel had a transverse scale of 1.95 mm. During random placement of the points within the array, points where allowed to overlap. The number of overlaps for each pixel within the array was equated to the aperture at that pixel and each unit of overlap was given a physical size of a micron. This created a fracture void geometry with transverse correlation lengths approximately equal to 7.8 mm and with a log-normal aperture distribution [Nolte and Pyrak-Nolte, 1991]. The aperture distributions were used to study the flow and deformation properties of the initial 512×512 aperture array and then subsectioned (Figure 1) down to 32×32 subsection (or scales from 1, $1/2$, $1/4$, $1/8$, $1/16$, and $1/32$ m) to study the effect of scaling on the flow-stiffness relationship. One hundred fractures were simulated at each scale to form the ensemble average values. The fluid flow calculations assumed the properties of water with the viscosity of 0.001 Pa s. The elastic properties of granite were assumed for the bulk rock (i.e., a Poisson ratio of 0.25 and Young’s modulus of 60 GPa [Jaeger et al., 2007]).

[8] The generated fractures were numerically deformed under a normal load [Hopkins, 1990]. Each asperity was modeled as a standing cylinder, and the normal load was

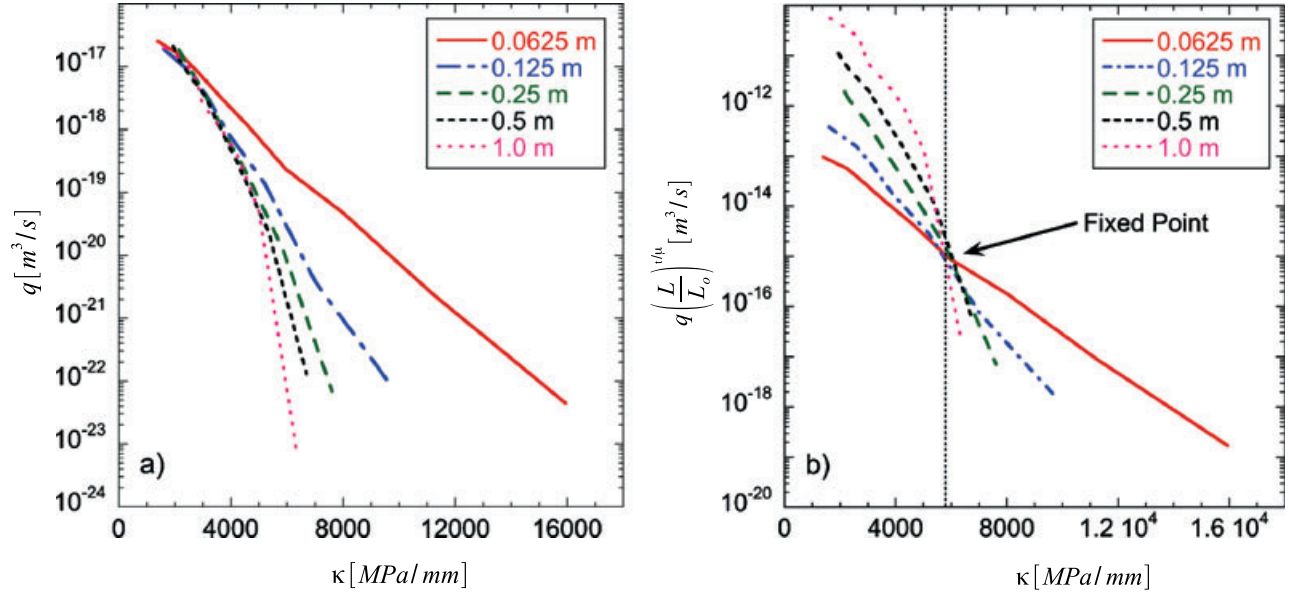


Figure 2. (a) Raw flow-stiffness data, averaged for each scale. (b) A partial data collapse of the flow-stiffness relationship. The flow rate was scaled by $(L/L_0)^{1/\mu}$.

applied to an infinite half-space. Both the cylinders and the half-space were given the same material properties (that of granite), and both were allowed to deform elastically. Numerically, this system is represented by a set of linear equations, with each equation computing the deformation of a given asperity. The number of equations grows as the contact area of the fracture grows. The method was improved by iteratively solving the linear system and using the fast multipole method to speed up the matrix-vector multiplication [Pyrak-Nolte and Morris, 2000]. The solver was modified to use periodic boundary conditions [Lambert, 1994] to remove edge effects. The deformation model provides the fracture displacement as a function of stress. The ratio of the increment of stress to an increment of displacement defines the fracture specific stiffness.

[9] Fluid flow rates were computed at each step in normal load by converting the aperture distribution to a network of elliptical pipes [Tran, 1998; Yang et al., 1989; Cheng et al., 2004]. Ellipses were used to match the variation in aperture (row-wise) and then connected in the direction of the pressure gradient. The analytic solution to laminar flow in an elliptical pipe was used to generate a system of equations that represented the flow through the fracture plane. This model is preferred over a bi-lattice grid method, because it is computationally more efficient (run-times are 4–10 times faster) and it was shown to model 2D micro-model experimental data more accurately [Cheng et al., 2004]. Figure 1b shows the fluid velocity field under a small load (0.6 MPa), while Figure 1c shows it under a large load (2.7 MPa) where the “critical necks” of the fracture geometry are clearly apparent.

3. Hydromechanical Finite-Sized Scaling

[10] The computed flow-stiffness relationships are shown in Figure 2a. Each curve represents a different physical scale. The finite-size effects are observed as a fan of curves when stiffness increases. The dynamic flow exponent, t , must be

determined to unravel the scaling function in equation (1), because it plays a key role in the first stage of the data collapse. This was completed by extrapolating the flow rate at threshold to the infinite size limit [Reynolds et al., 1980]. To extract the exponent, a power law is fit to the flow rate at threshold for each scale as a function of scale and provides the critical exponent. The flow exponent was determined to be $t/\mu = 2.38$. In Figure 2b, the data are partially collapsed by scaling the flow rate by $(L/L_0)^{1/\mu}$, reflecting the pre-factor of the scaling function in Equation (1). This scaling also displays the fixed point near 5800 MPa/mm, where each of the flow-stiffness curves cross at a single point, meaning that

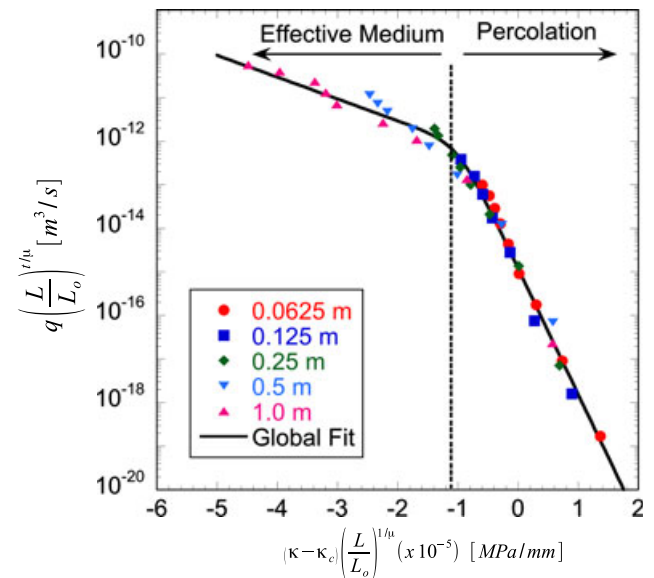


Figure 3. Universal flow-stiffness function showing a full data collapse. The solid line is provided to guide the eye. The break in slope divides the effective medium regime from the percolation regime.

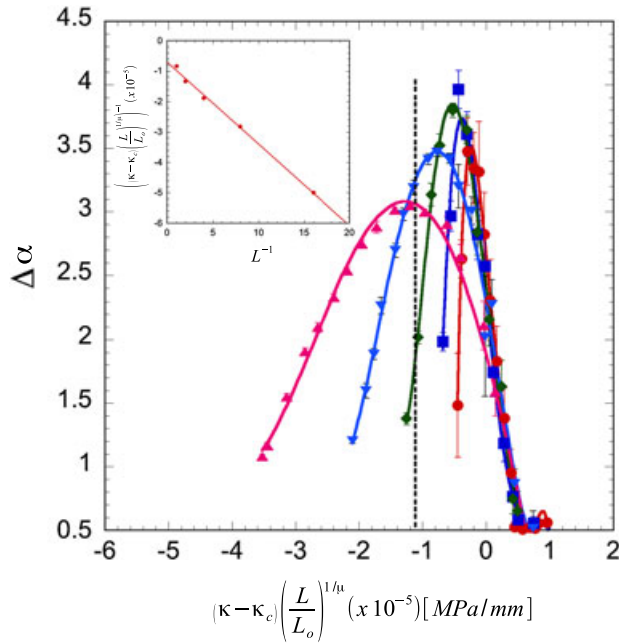


Figure 4. Width of the multifractal spectrum plotted against the scaled fracture stiffness. Lines are provided to guide the eye. The inset shows the extrapolation of the peak location to the infinite scale. The symbols and line colors are the same as those in Figure 3.

flow and stiffness are scale invariant at that point. The stiffness at this fixed point is defined as the critical stiffness, κ_c , used in equation (1) and is also the average stiffness at the critical threshold. This value of critical stiffness is a key parameter in the second and final stage of data collapse.

[11] To complete the data collapse, the stiffness axis was shifted by κ_c and scaled by $(L/L_0)^{1/\mu}$, as shown in Figure 3, while continuing to use $q(L/L_0)^{t/\mu}$ as the scaled vertical axis. With this scaling, all the data at all scales fall on a single curve that has two clear regions with distinct slopes. The solid line on Figure 3 is shown to guide the eye and represents the scaling function of equation (1). There is a clear break in slope near the abscissa value of -1 , with each region above and below this value displaying an exponential dependence. The curve has a slope of -2 for greater values of the abscissa and a slope of -0.5 for lesser values.

[12] It was observed that the flow velocity field changed its character from *sheet-like* to *string-like* patterns with increasing stress. The break in the scaling function's slope was roughly associated with this change in morphology. To test this association, we performed a multifractal analysis on the fluid velocity fields. A multifractal is a collection of sets with differing fractal dimensions, and the width of the multifractal spectrum captures the heterogeneity of these sets [Feder, 1988]. To calculate the multifractal spectrum, a box counting method [Feder, 1988; Nolte and Pyrak-Nolte, 1991] was used that depends on the scale and the mass moment. At low stresses, the width $\Delta\alpha$ of the fractal spectrum is small, and the geometry of the fluid speeds exhibits mono-fractal behavior because their statistical moments are distributed nearly homogeneously across the fracture plane. As normal stress increases, the width of the spectrum increases as the moments become inhomogeneous up to stresses associated with the break in slope at

$(\kappa - \kappa_c)(L/L_0)^{1/\mu} = -10^{-5}$ MPa/mm. At stresses above the break, the multifractal spectrum decreases because the fractures enter the critical regime and the fluid speed is dominated by the “critical necks.” The break in slope of the scaling function occurs when the width of the multifractal spectrum is at a maximum (Figure 4). The shift in the peaks is a finite-size effect. The subplot of Figure 4 extrapolates the inverse of the scaled stiffness, derived from the positions of the peaks of the spectra, to the infinite size limit. The peak extrapolates to -1.42×10^{-5} MPa/mm, which matches the observed break in the scaling function.

4. Discussion

[13] The scaling of the data displayed in Figure 3 is an important result that connects the hydraulic properties of a weakly correlated fracture (correlation length ≈ 8 mm relative to 1 m sample size) to the fracture specific stiffness; a property that can be probed using remote seismic techniques. The local geometric properties of the system, i.e. “critical necks,” were captured by a scaling function that depends on the global transport critical exponent, t , and the critical stiffness which allowed the system to be written in a scale invariant form. Furthermore, percolation theory was used to derive the geometric scaling exponents from the static cluster statistics of generated fractures. The normal load becomes a key control variable in this study. When the load changes, contact areas are created that alter the cluster statistics of the fracture under load. Rather than the geometry of a fracture completely determining hydraulic properties, the deformation under load must be considered. Thus, fracture specific stiffness can stand in for the void/contact areas, because the stiffness reflects the current state of the topology under the given load conditions.

[14] The system under consideration contains both hydraulic and mechanical properties, and therefore possibly two non-trivial scaling properties. It is well known that the flow rate enters a critical scaling regime near the percolation transition [Stauffer and Aharony, 1985]. Conversely, the criticality of the mechanical properties were studied and found to have simple scaling with void area fraction. Because of this, a global mechanical scaling exponent is not required to complete the full data collapse, leaving the entire system dependent on the transport exponent, t . This also means that the fracture specific stiffness can replace the void area fraction as a surrogate, making a strong connection to seismic monitoring techniques.

[15] The two exponential regions in the scaling function were important results from this study. At low stresses, the flow field across the fracture plane is homogeneous. For example, by subsectioning the field in Figure 1b into smaller regions, the fluid velocity profiles of each subsection will be similar. This implies that the flow covers most of the void spaces of the fracture and is more *sheet-like*. In the limiting case, where the contact area fraction reduces to zero, the flow rate returns to the “cubic law” and the deformation of the apertures can be estimated by conserving the volume of the bulk rock [Pyrak-Nolte et al., 1988]. As stress increases, flow paths begin to close, leaving only the main backbone of the original paths. At high stresses, many regions of the void space are without flow leaving only narrow channels that contain flow. Therefore, the change in slope can be understood as a transition from *sheet-like* to *string-like* topology.

5. Conclusion

[16] From this analysis, we conclude that the geometry of a fracture provides all the necessary information to define a scaling relationship between the fracture specific stiffness and the flow rate for weakly correlated fracture aperture geometries. By conducting a finite-size scaling analysis, we were able to describe the localized fracture properties with a global flow scaling exponent, t . Incorporating the fracture specific stiffness as a surrogate for void area fraction within the framework of standard percolation theory enabled us to describe the flow-stiffness relationship of fractures with a single scaling function. We have demonstrated that the change in slope in the scaling function is related to the multifractal spectrum width of the flow speed distribution. However, the values for the slopes of the effective medium and critical regimes remain to be explained. Nonetheless, this scaling function provides a stepping-stone to a non-intrusive method to probe the hydraulic properties of single rock fractures in the subsurface. This could provide new methods to determine the future success of subsurface projects. Extending the results here and understanding how stronger correlations affect the scaling is of utmost important because correlated void geometries are often found in nature [Brown *et al.*, 1986; Pyrak-Nolte *et al.*, 1997]. This is a subject of continuing research.

[17] **Acknowledgments.** This work is supported by the Geosciences Research Program, Office of Basic Energy Sciences US Department of Energy (DEFG02-97ER14785 08, DE-FG02-09ER16022), by the Geo Mathematical Imaging Group at Purdue University, the Purdue Research Foundation, and from the Computer Research Institute At Purdue University.

[18] The Editor thanks one anonymous reviewer for his/her assistance in evaluating this paper.

References

- Brown, S., R. Kranz, and B. Bonner (1986), Correlation between the surfaces of natural rock joints, *Geophys. Res. Lett.*, *13*(13), 1430–1433.
- Cheng, J., J. Morris, J. Tran, A. Lumsbaine, N. Giordano, D. Nolte, and L. Pyrak-Nolte (2004), Single-phase flow in a rock fracture: Micro-model experiments and network flow simulation, *Int. J. Rock Mech. Min.*, *41*, 687–693.
- Feder, J. (1988), *Fractals*, pp. 85–88, Plenum Press, New York.
- Hopkins, D. L. (1990), The effect of surface roughness on joint stiffness, aperture, and acoustic wave propagation, Ph.D. thesis, University of California at Berkeley, Berkeley, Calif.
- Jaeger, J., N. Cook, and R. Zimmerman (2007), *Fundamentals of Rock Mechanics*, 4th ed., pp. 365–394, Wiley-Blackwell, Hoboken, N.J.
- Lambert, C. (1994), Multipole-based algorithms for efficient calculation of forces and potentials in macroscopic periodic assemblies of particles, Ph.D. thesis, Duke University, Durham, N.C.
- Nolte, D., and L. Pyrak-Nolte (1991), Stratified continuum percolation—Scaling geometry of hierarchical cascades, *Phys. Rev. A*, *44*(10), 6320–6333.
- Pyrak-Nolte, L. J., and J. P. Morris (2000), Single fractures under normal stress: The relation between fracture stiffness and fluid flow, *Int. J. Rock Mech. Min.*, *37*, 245–262.
- Pyrak-Nolte, L., L. Myer, N. Cook, and P. Witherspoon (1987), Hydraulic and mechanical properties of natural fractures in low permeability rock, in *Proceedings of the 6th International Congress on Rock Mechanics*, Montreal, Canada, pp. 225–231, Balkema, Rotterdam, The Netherlands.
- Pyrak-Nolte, L. J., N. G. Cook, and D. D. Nolte (1988), Fluid percolation through single fractures, *Geophys. Res. Lett.*, *15*(11), 1247–1250.
- Pyrak-Nolte, L. J., C. D. Montemagno, and D. D. Nolte (1997), Volumetric imaging of aperture distributions in connected fracture networks, *Geophys. Res. Lett.*, *24*(18), 2343–2346.
- Renshaw, C. E. (1995), On the relationship between mechanical and hydraulic apertures in rough-walled fractures, *J. Geophys. Res.*, *100* (B12), 24,629–24,636.
- Reynolds, P., H. Stanley, and W. Klein (1980), Large-cell Monte Carlo renormalization group for percolation, *Phys. Rev. B*, *21*(3), 1223.
- Stauffer, D., and A. Aharony (1985), *Introduction to Percolation Theory*, pp. 60–73, CRC Press, Philadelphia, PA.
- Tran, J. (1998), Efficient simulation of multiphase flow in three-dimensional fracture networks, Ph.D. thesis, University of Notre Dame, Notre Dame, IN.
- Walsh, J. B. (1981), Effect of pore pressure and confining pressure on fracture permeability, *Int. J. Rock Mech. Min.*, *18*(5), 429–435.
- Walsh, J. B., and M. A. Gosenbaugh (1979), New model for analyzing the effect of fractures on compressibility, *J. Geophys. Res.*, *84*(B7), 3532–3536.
- Witherspoon, P. A., J. S. Y. Wang, K. Iwai, and J. E. Gale (1980), Validity of cubic law for fluid-flow in a deformable rock fracture, *Water Resour. Res.*, *16*(6), 1016–1024.
- Yang, G., N. Cook, and L. Myer (1989), Network modelling of flow in natural fractures as a guide for efficient utilization of natural resources, *Proc. of 30th US Symposium on Rock Mechanics*, 57–64, Morgantown, W.V.
- Zimmerman, R. W., and G. S. Bodvarsson (1996), Hydraulic conductivity of rock fractures, *Transport in Porous Media*, *23*(1), 1–30.
- Zimmerman, R. W., D. W. Chen, J. C. S. Long, and N. G. W. Cook (1990), *Hydromechanical Coupling between Stress, Stiffness, and Hydraulic Conductivity of Rock Joints and Fractures*, *Rock Joints*, pp. 571–577, Balkema, Rotterdam, The Netherlands.